Impact of Nanowires on the Properties of Magnetorheological Fluids and Elastomer Composites

R. C. Bell[1], D. T. Zimmerman[1], and N. M. Wereley[2]
[1]The Pennsylvania State University, Altoona College
[2]University of Maryland
USA

1. Introduction

Magnetorheological (MR) fluids are a type of smart material whose effective viscosity may be rapidly changed (~few ms) in a nearly reversible manner by the application and removal of an externally-applied magnetic field. Conventional MR fluids are composed of micron-scale, ferromagnetic spherical particles (typically 30 to 40 volume percent) suspended in a hydrocarbon, silicone, or aqueous carrier fluid (Klingenberg, 2001). The viscosity and apparent shear strength of these suspensions can be controlled by varying the strength of an applied magnetic field. Without an applied magnetic field (off-state), MR fluids are a viscous liquid/particle suspension with a viscosity in the range of 0.1 – 3 Pa · s. Upon application of a magnetic field (on-state), the particles acquire a magnetic polarization and attract one another forming chain-like structures that join to form columnar structures parallel to the applied field (schematic, Fig. 1). The newly formed columns span the surfaces of the device parallel to the field lines resulting in a material that behaves as a Bingham plastic fluid, with increased viscosity and apparent yield stress under shear. The viscosity and yield stress of the fluid is scalable with the magnitude of the applied magnetic field until magnetic saturation of the particles is reached (Jones & Saha, 1990). At high fields, the fluid is converted to a semi-solid with a five to six orders-of-magnitude change in apparent viscosity (Genç & Phulé, 2002). As the particle loading approaches 40 vol. %, the field-induced yield stress can reach 100 kPa. Exceeding the yield stress of the fluid causes the fibril chains and columnar structures to continuously break and re-form, resulting in a post-yield viscosity.
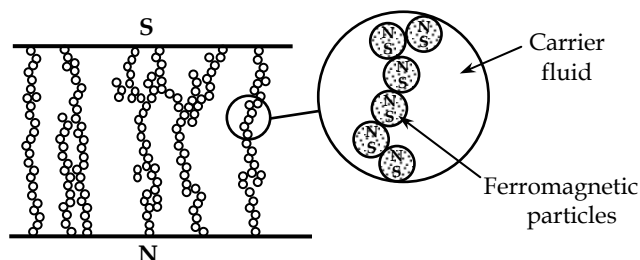

Fig. 1. Schematic representation of the magnetorheological effect with spherical particles.

The rheological properties of MR fluids depend not only on the strength of the applied magnetic field, but also on the loading (vol. % or wt. %), size, composition, magnetic properties, and morphology of the particles, as well as on the concentration and type of additives within the suspension. As the applied magnetic field is increased, the shear strength of the fluid eventually reaches a maximum as the magnetization saturation of the particles is reached. Particle loading is the most important factor affecting the achievable yield strength of MR fluids. While increasing the volume fraction of particles in the suspension results in an increase in the yield strength of the material, it also results in an increase in the off-state viscosity. The shear strength of the suspensions increases with an increase in size of the particles (Genç & Phulé, 2002); however, spherical particles larger than about 10 µm tend to settle rapidly, even with the addition of special additives. Suspensions composed of nanometer-sized particles tend to settle more slowly, if at all, due to Brownian motion. However, the effectiveness of Brownian motion combined with a smaller magnetic moment, also hinders the formation of the chain-like structures in these energized fluids, greatly reducing the yield stress of the material (Rosenfeld et al., 2002; Poddar et al., 2004; Chaudhuri et al., 2005). Given these competing factors, the ideal diameter of particles is in the range of 1 to 10 µm. In this size range, sedimentation still occurs due to the inherent density difference between the particles and the carrier fluid. Upon settling, the particles tend to form tightly packed sediments resulting from remnant magnetization within the particles and are not easily re-dispersed (Phulé & Ginder, 1998). Since the yield stress of MR fluids is directly related to the volume fraction of particles in the suspension, the behavior of the fluid is less predictable during this remixing period. The settling rate can be reduced slightly and less dense sediments formed, by the addition of special additives such as surfactants, nanoparticles, and other non-spherical particles (Poddar et al., 2004; Chaudhuri et al., 2005; Chin et al., 2001; Weiss et al., 1997; Wereley et al., 2006).

There are a growing number of applications that exploit the MR fluid's continuously controllable, field-dependent yield stress including variable dampers, brakes, clutches, and optical polishing machines (Kamath et al., 1999; Zipser et al., 2001; Ramallo et al., 2002; Harland et al., 2001; Kordonski et al., 2006). Conventional MR fluids have had some difficulty finding widespread commercial use, owing to relatively high manufacturing costs, as well as a limitation on the volume loading necessary to maintain their low off-state viscosity. The use of MR fluids in more diverse applications have been limited, due to the settling of the particles in the absence of continual mixing (Chen & Chen, 2003) and particle wear (Carlson, 2003) that tends to reduce the efficacy of the fluid over time and eventually lead to device failure.

Both the yield stress and settling properties of magnetorheological fluids have been shown to depend on particle morphology; however, few studies have explored the particle shape-dependence in either MR fluids (Chin et al., 2001; Nishiyama et al., 2005; Kuzhir et al., 2009; López-López et al., 2009) or electrorheological (ER) fluids (Kanu & Shaw, 1998; Lengálová et al., 2003; Sanchis et al., 2004; Yin & Zhao, 2006). Studies involving electrorheological fluids utilizing elongated titanate (TiO_2) whiskers demonstrated greatly reduced sedimentation. Moreover, with a 10 vol. % loading, these fluids displayed an increase in yield stress from 80 to 1100 Pa when ~80 nm diameter particles were exchanged with TiO_2 whiskers (with 10 nm diameters by several hundreds or thousands nanometers) (Yin & Zhao, 2006). However, it is unclear whether the increase in yield stress was due to the differences in particle morphology or due to the large mass differences between the particles. Studies on MR fluids

with up to 7 vol. % 60 µm long, 4.8 µm diameter cobalt microfibers displayed substantial mitigation of sedimentation and an increase in yield stress as compared to suspensions containing 1.34 µm diameter cobalt spheres (López-López et al., 2009). It was suggested that the enhancement of the yield stress was due to inter-fiber solid friction. Yet, the fibers used in these studies had non-uniform dimensions, rough surfaces, and the difference in the size of the particles made a direct comparison between the properties of the two types of suspensions difficult to interpret. All of these studies suffered from broad size distribution, inconsistency in particle shape, surface roughness, and particle fragility, making it difficult to form conclusions or infer the underlying physics. Thus, while MR/ER fluids employing elongated particles demonstrated reduced sedimentation properties, the effect on yield stress remained unclear.

More recent studies utilizing nanowires have shown promising results for not only reducing or preventing settling, but have also increased the apparent yield stress of the materials (Bell et al., 2007; Bell et al., 2008; Ngatu et al., 2008; Zimmerman et al., 2009). Unlike the ferromagnetic oxide particles used in previous studies (Chin et al., 2001) and those formed from spherical particles adjoined in the presence of a magnetic field (López-López et al., 2009), nanowires have well defined structure and controllable length distributions. This facilitates systematic experimental and theoretical studies and will lead to increased understanding and design control. Nanowire-based MR fluids have two distinct advantages over suspensions that contain only spherical particles (Bell et al., 2007; Bell et al., 2008; Ngatu et al., 2008). First, the maximum achievable yield stress can be twice that of conventional fluids (or greater, even at the same metal loading) and nanowire-based fluids also provide more sensitive control over the yield stress at field strengths below magnetic saturation of the suspension. Second, sedimentation is greatly reduced, if not eliminated. However, one drawback to pure nanowire fluids is the limit on particle loading to 10 vol. %, resulting in fluids with a maximum yield stress much lower than most conventional MR fluids. The wires occupy a much larger effective volume compared to spheres, due to the excluded volume concept. Even so, fluids using only nanowires display some very interesting and useful properties. For applications that require the highest yield stress (and thus maximum particle loading of 35-40 vol. %), a "dimorphic" fluid was generated that contains both spherical and nanowire particles. These fluids not only display reduced sedimentation, but some formulations also display an increase in yield stress over conventional fluids.

2. Synthesis of magnetorheological fluids

Two types of ferromagnetic particles were used in this study. To replicate conventional MR fluids, we used spherical iron particles having diameters of 1 - 3 µm or 6 - 10 µm (Alfa Aesar), cobalt particles with nominal diameters of 1.6 µm (Alfa Aesar), and nickel particles with diameters in the range of 1 to 10 µm (Novamet). Nanowire-based fluids were synthesized using wires generated via template-based electrodeposition techniques.

2.1 Nanowire generation and characterization
The nanowires were generated via template-based electrodeposition using commercially available, anodized alumina membranes (Whatman) as templates and various electrolytic solutions depending on nanowire composition. The electrolyte solution for nickel nanowires consisted of 1.1 M NiSO$_4$, 0.19 M NiCl$_2$, and 0.6 M H$_3$BO$_3$, with the pH of the solution

adjusted to 3.5 using H_2SO_4. A 99.5% nickel foil was used as the working electrode. Iron nanowires were fabricated using an electrolytic solution consisting of 0.9 M $FeSO_4$, 0.03 M $FeCl_2$, 0.10 M NH_4Cl, 0.01 M $C_6H_8O_6$, and 0.5 M H_3BO_3 at a pH of 3 using H_2SO_4. A 99.99% iron foil was used as the working electrode. Cobalt nanowires were generated from a solution containing 0.2 M $CoSO_4$, 0.02 M $CoCl_2$, and 0.3 M H_3BO_3 adjusted to a pH of 3.5 using H_2SO_4. A 99.97% cobalt foil was used as the working electrode. The working electrodes were suspended approximately 2 cm from the alumina template in the electrolytic solutions. Wires were electrodeposited using a current density ranging from 4.8-5.5 mA cm^{-2} under ambient conditions without agitation. The diameter of the wires was fixed by the diameter of the channels within the membrane and the lengths of the wires were controlled by the current and deposition time. The nanowires were recovered by dissolving the wire-filled templates in a 1 M NaOH solution.

Particle dimensions and size-distribution information for both the spherical particles and nanowires were obtained using Hitachi S570 and Hitachi S800 scanning electron microscopes (SEM). Hundreds of images were examined to determine an average and standard deviation for the diameter and length. The size distribution of the wires can be seen in the SEM micrographs in Fig. 2.

Using induction-coupled plasma spectrometry (ICP), the stoichiometric purity of all wire compositions was determined to be greater than 99.4%. In particular, the ICP data indicates that the wires do not contain significant amounts of gallium, indium, copper, aluminum, or other elements that come in contact with the wires during fabrication.

The coercivity, remanence, and magnetic saturation all influence the magnetorheological properties of the fluids and depend on the composition and aspect ratio of the particles. The magnetic properties of the particles and MR fluids were determined at room temperature using a Lakeshore 7400 series vibrating sample magnetometer (VSM). Figure 3 shows hysteresis curves exhibited in iron nanowires aligned parallel to one another within an alumina template, where the easy axis is parallel to the field flux and the hard axis is perpendicular to the flux. This reveals a shape-anisotropy in the wires due to their aspect
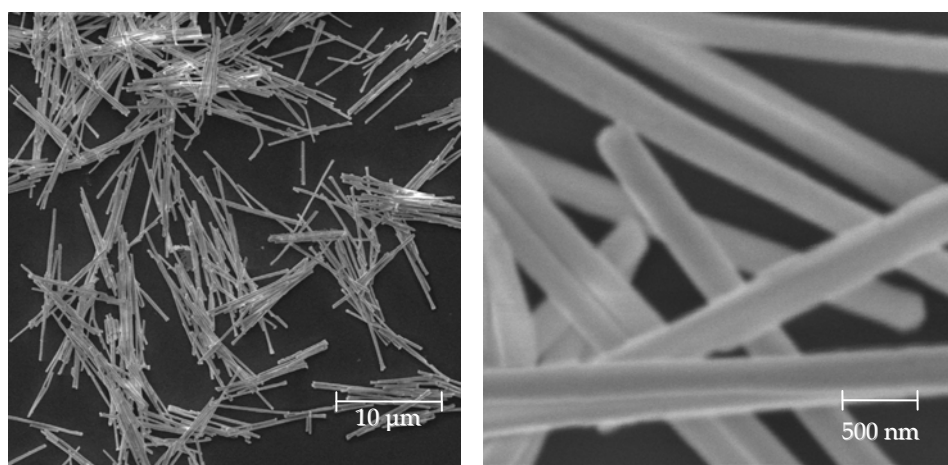

Fig. 2. SEM micrographs of 6.8 ± 1.7 µm long cobalt nanowires with diameters of 296 ± 39 nm.
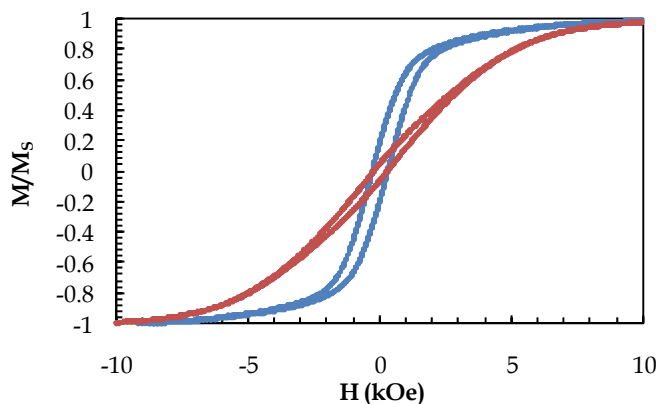
Fig. 3. VSM measurements for 7.89 µm iron nanowires still contained within the alumina template and therefore aligned parallel to one another. Wires aligned parallel to the field are represented by the red curve and wires aligned perpendicular to the field are represented by the blue curve.

ratio. This anisotropy causes the suspended wires within an MR fluid to experience a torque when exposed to the slightly non-uniform magnetic field, resulting in the self-aligning behavior of the nanowires discussed in *section 3.2*. Since the saturation magnetization (M_S) is obtained when all magnetic moments in the material are aligned in the same direction, it is an intrinsic material property which is unrelated to sample morphology. Therefore, we would expect both the spheres and nanowires to have a value that is relatively similar to the bulk material of the same composition. The magnetic saturation of the iron spheres and nanowires is 200.8 emu cm^{-3} and 174.1 emu cm^{-3}, respectively. When both are assumed to have a bulk density, the magnetic saturation for cobalt spheres is 126.3 emu g^{-1} and for the nanowires, it drops to 111.6 emu g^{-1}. This deviation from the bulk value is not surprising due to the oxide layer that is present. It is not unexpected that the nanowires would display a lower value due to increased surface area and the concomitant increase in oxide. As expected, spherical iron particles exhibit a near zero coercivity.
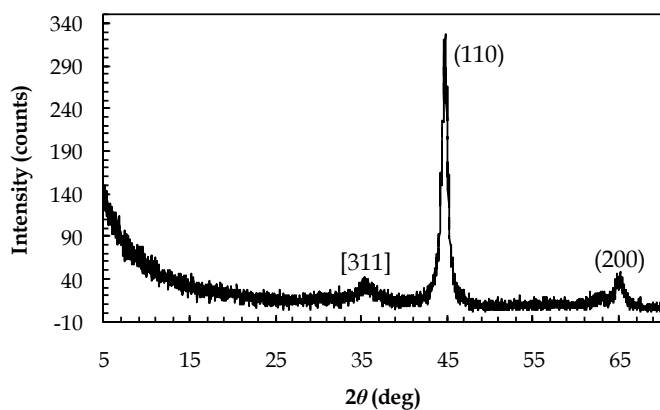

Fig. 4. XRD of 8.7 ± 2.7 µm long by 318 ± 51 nm diameter iron wires. The lattice planes for iron are indicated in ( ) brackets and those resulting from the oxide layer are indicated in [ ] brackets.

To determine the bulk crystal structure and approximate grain size of the crystallites forming the spheres and nanowires, x-ray diffraction (XRD) patterns are acquired using a Scintag X2 automated diffractometer equipped with a Peltier solid-state detector. XRD of the free wires indicates that iron wires grow in a bcc polycrystalline structure and that cobalt wires grow in a hexagonal polycrystalline structure. Using Scherrer's formula, the approximate crystallite size for as-deposited wires was determined to be 23.8 nm, 14.8 nm, and 42.2 nm for the nickel, iron, and cobalt, respectively. The XRD revealed the susceptibility of the iron nanowires to oxidation (some samples display a composition as high as 28% iron oxide) while those of nickel and cobalt displayed only minor peaks (or none at all) for their corresponding oxides. We observed minor metal oxide peaks for the iron spherical particle distributions, but none for those of nickel or cobalt.

2.2 Magnetorheological fluid composition

The MR fluids were prepared by thoroughly mixing the ferromagnetic particles in silicone oil. Lecithin was added to the oil prior to the addition of particles as a surfactant for producing good dispersions with 2 wt. % total particle mass. For the nickel-based MR fluids, the particles were suspended in 0.2 Pa·s silicone oil (Alfa Aesar). Magnetorheological fluids used for the percolation studies (*Section 4*) were prepared using a 0.45 Pa·s viscosity silicone oil. A more viscous fluid was used for these low vol. % suspensions to avoid sedimentation and to prevent the oil from being expelled from the rheometer. All other MR fluids were prepared using a 0.18 Pa·s viscosity silicone oil (GE SF96-200).

2.3 Rheological fluid testing

To determine the flow curves (shear stress vs. shear rate), measurements were carried out on an Anton-Paar Physica MCR300 parallel plate rheometer equipped with a MRD180 magnetic cell. A standard gap of 1 mm was maintained between the plates and a nominal 0.3 mL sample of fluid was placed between them. A Hall probe (F.W. Bell FH301) was placed within the gap to calibrate the electromagnet current of the rheometer in terms of the magnetic flux density within the fluid-containing gap. For the percolation studies, a gap of 0.5 mm was maintained between the plates and a nominal 0.15 mL sample of fluid was used. A magnetic flux density from 0 to 1.0 T was used for the various studies and the temperature of all samples was maintained at 25°C with a closed-cycle cooling system. To avoid sedimentation, the tests were started as soon as the thoroughly-mixed fluid was injected between the disks.

For the preliminary studies of the nickel nanowire-based MR fluids, a custom built rheometer was constructed. This device consisted of a C-shaped electromagnet capable of generating fields up to 0.6 T as measured by a Hall probe between the poles of the magnet. The sample was then placed tightly between the poles. To measure effective viscosity, a thin aluminum plate was submersed 1.3 cm into the fluid with 1 mm of the MR fluid on either side of the plate. With the magnetic field applied, a force transducer (range of 0.02 – 45 N) measured the force required to pull the plate out of the fluid at a rate of 1.06 mm/s. However, due to the poor resolution of this force transducer, the maximum field of 0.6 T was necessary to measure the yield stress within a reasonable uncertainty. Thus, all future studies were conducted on the aforementioned Anton-Paar rheometer.

2.4 Sedimentation testing

The sedimentation velocity of particles within the suspensions was determined by exploiting the magnetic properties of MR fluid particles. As seen in Fig. 5, the inherent density difference between the carrier fluid and magnetic particles results in sedimentation of the particles, leaving a volume of supernatant fluid (the clarified fluid above the sediment mudline). To quantify and compare the sedimentation velocity of conventional sphere-based MR fluids with those containing nanowires, an inductance-based solenoid sensor was constructed to track the mudline location of the settling fluid (Ngatu & Wereley, 2007). The sedimentation velocity is defined as the rate at which the mudline descends due to particle settling, until the particles pack tightly at the bottom of the vial without further sedimentation. The magnetic permeability of the MR fluid is highly dependent on the volume fraction of fluid. Therefore, the inductive sensor solenoid is maintained within this region. The permeability of the MR fluid within the sensor region is related to the sensor inductance L as

$$L = \frac{N^2 A \mu_0}{l} \mu_r \tag{1}$$

where N is the number of turns of the solenoid, A is cross-sectional area of the coil, l is solenoid length, μ_0 is the vacuum permeability, and μ_r is relative permeability of the MR fluid. Thus, the rate of change of the mudline can be determined as it traverses through the sensor by measuring the rate of change of magnetic inductance within the sensor.

Another method to quantify the sedimentation properties of fluids is the percentage of sedimentation, θ, given by

$$\theta = \left(\frac{\text{volume of supernatant fluid}}{\text{total volume of fluid}} \right) \times 100\% \tag{2}$$

The percentage of sedimentation is an indication of how tightly-packed the particles become once settled and is directly related to the ease with which the suspensions can be re-dispersed.
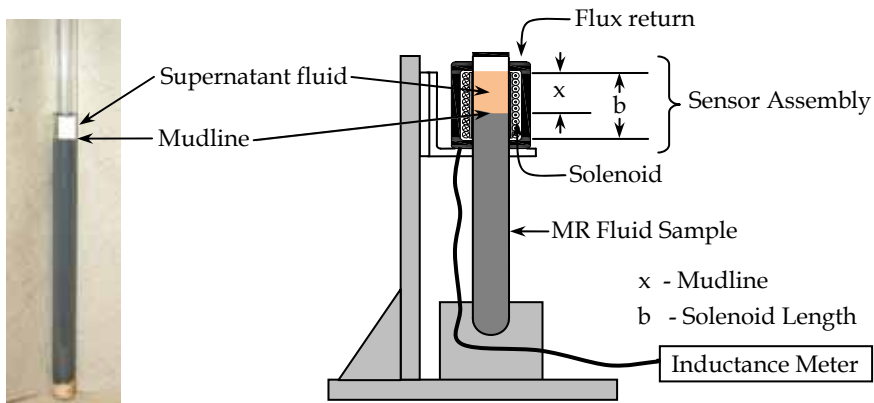

Fig. 5. Sedimentation testing apparatus for determining settling velocity of MR fluids. The inductance measuring instrument is comprised of the sensor assembly, an inductance meter, and a stand to mount the apparatus and sample.

3. Nanowire-based magnetorheological fluids

3.1 Nickel-based MR fluids

To investigate the feasible performance of the new nanowire-based MR fluids, we conducted a preliminary investigation of the rheological properties and settling characteristics of fluids containing nickel nanowires with an average length of 5 – 25 µm and diameters of 300 ± 30 nm (Bell et al., 2007). Using the custom-designed rheometer described in section 2.3, the rheological properties of these fluids were compared to conventional fluids containing nickel-carbonyl spheres (range of 1-10 µm dia.) having the same volume percent of suspended particles. The rheological and settling properties of the MR fluids consisting of 7.6 vol. % nickel nanowires were compared to fluids containing 7.6, 17.5, and 40.0 vol. % nickel spheres. These initial studies indicated that there was no difference in the maximum yield stress of the suspensions. However, the settling properties of the fluids were significantly different. The nanowire-based fluids displayed no settling after several months (discussed further below). However, these studies suffered from several shortcomings. The custom-built rheometer lacked the sensitivity to examine fluids below magnetic saturation and could not measure the rheological properties at high shear rates. In addition, the wires were not well-characterized and an average wire length could not be determined from the limited SEM images acquired for this study. However, the settling results were so promising that these initial studies paved the way for more carefully constructed fluids using instrumentation capable of examining the rheological and sedimentation properties with greater sensitivity.

3.2 Iron-based MR fluids

We then focused our attention on iron nanowire-based MR fluids with two distinct length distributions: 5.4 ± 5.2 µm and 7.6 ± 5.1 µm with diameters of 260 ± 30 nm. These were compared with conventional sphere-based MR fluids (Bell et al., 2008). These studies illustrated the distinct differences between conventional MR fluids employing spherical particles to nanowire-based fluids with the same ferromagnetic material and particle loading.

The rheological properties of the fluids were determined using the parallel plate rheometer modified with an electromagnet to allow application of a variable magnetic field across the sample. We plotted steady-state flow curves of shear stress (τ) versus shear rate ($\dot{\gamma}$) as seen in Fig. 6. A Bingham-plastic (BP) constitutive model (Jolly et al., 1999) was used to fit the flow curve to determine the apparent yield stress (τ_y) and the post-yield viscosity, η. The BP model for the viscoplastic flow with yield stress is given by

$$\tau = \tau_y + \eta\dot{\gamma} \qquad (\dot{\gamma} > 0) \tag{3}$$

The values of τ_y and η were determined by fitting with a weighted least-squares-error minimization for each fluid tested at all values of the applied field. By using the measured shear rates as the weighting factor, the model provided a better fit to the high shear rate data.

As shown in Fig. 7, the dynamic yield-stress displays a dependence on the applied field for all the fluids studied. At a saturated magnetic flux density, it approaches a maximum value of 4.72 kPa for fluids containing 6 vol. % iron spheres. For fluids containing the 5.4 µm iron nanowires in silicone oil, we observed maximum yield stresses of 0.65, 2.23, and 4.76 kPa for the 2, 4, and 6 vol. % fluids, respectively. The yield stress increased to 8.23 kPa for the 6 vol. % fluid when the average length of the wires increased to 7.6 µm.
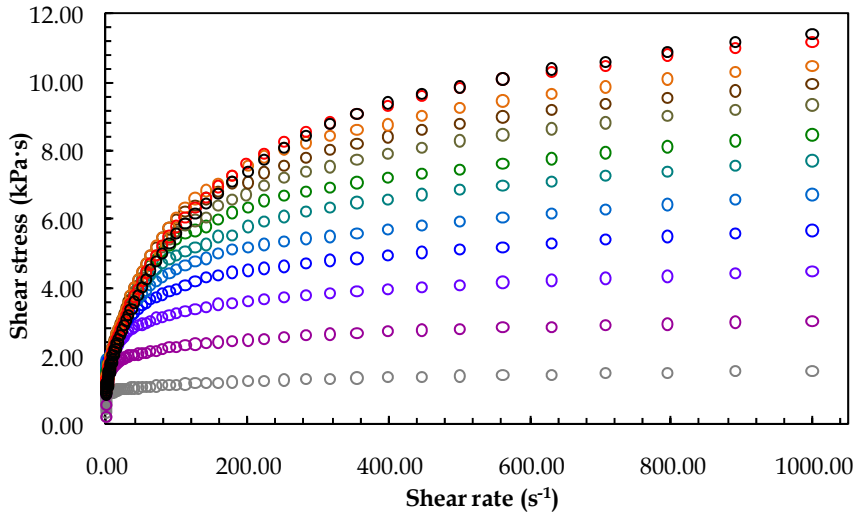
Fig. 6. Experimental flow curves for fluids containing 6 vol. % 7.6 µm Fe nanowires. The applied magnetic field was varied from 0.0 T (bottom) to 0.72 T (top).
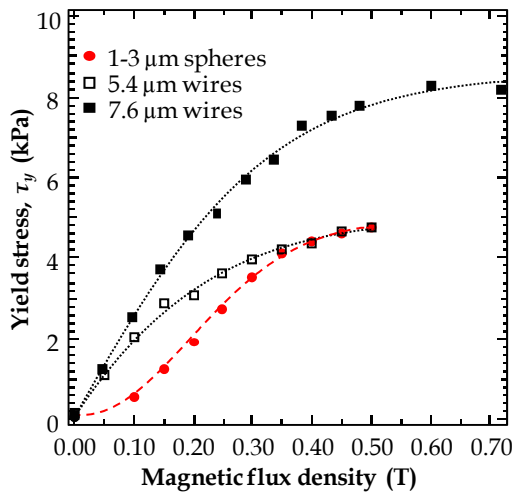

Fig. 7. Yield stress versus magnetic flux density for MR fluids containing 5.4 µm and 7.6 µm iron nanowires and for those fluids with 1 - 3 µm iron spheres. All fluids have a 6 vol. % particle loading. The dotted curves are included simply as a visual aid.

As seen in Fig. 7, the nanowire-based fluids exhibit a more sensitive response displaying a higher yield stress at low field as compared to the sphere-based fluids. This enhancement in the response is likely attributed to magnetic shape-anisotropy of the wires. The nanowires experience a torque within the applied magnetic field forcing them to align with their long axis parallel to field (Qi et al., 2003) and they experience a greater magnetization due to the shape anisotropy (Sun et al., 2005).

Models of the yield stress (τ_y) for sphere-based fluids predict a characteristic response at intermediate fields below saturation as given by

$$\tau_y \propto \phi\mu_0 M_S^{1/2} H^{3/2} \qquad (4)$$

where μ_0 is the permeability of free space, ϕ is the volume fraction, M_S is the magnetic saturation of the material, and H is the strength of the applied magnetic field. The sphere-based suspensions used in this study displayed similar behavior. However, for the nanowire-based suspensions, the trend in the yield stress is found to be proportional to the square root of the applied field,

$$\tau_y \propto \phi\mu_0 H^{1/2} \qquad (5)$$

How the magnetic saturation and shape anisotropy of the particles quantitatively affects the yield stress of the nanowire-based suspensions is still not well understood. The magnetic saturation of the nanowires is a function of their length and diameter, with longer wires (with fixed diameter) having a higher magnetic saturation (Han et al., 2002). Yet the difference in the magnetic saturation of the particles cannot account for the substantial difference in the yield stresses of the fluids containing the two wire lengths observed in our studies. Therefore, other factors such as magnetostatic coupling between neighboring wires (this tends to create a magnetic easy axis perpendicular to the wire axis), inter-fiber friction, and structural differences of the two types of suspensions in an applied magnetic field must also be considered. Some structural differences between sphere-based fluids and nanowire-based fluids are apparent in the SEM micrographs of Fig. 8.

Knowing the structure of the suspension both in the presence (on-state structure) and absence (off-state structure) of a magnetic field is essential to understanding the properties of these fluids. To generate these images, the wires were suspended in a drop of water and a uniform magnetic field was applied across the droplet. The droplet was then allowed to
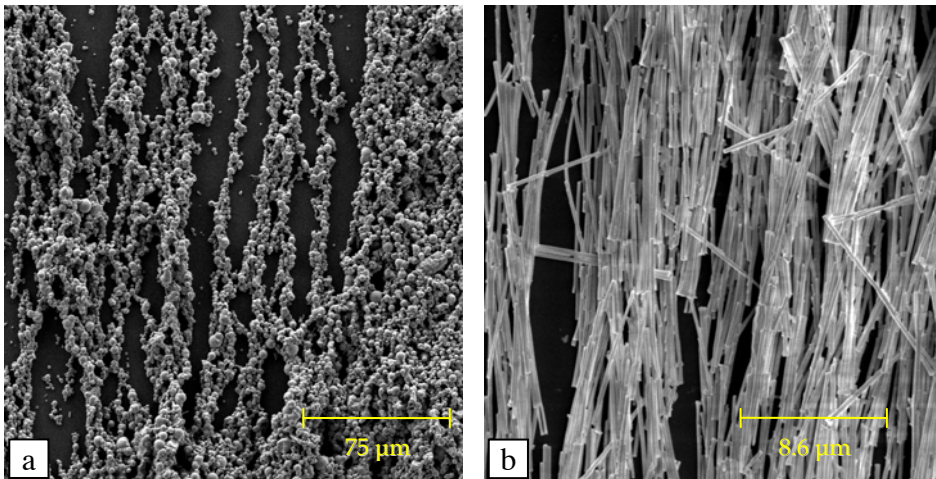

Fig. 8. SEM micrograph showing the columnar structures of (a) spherical 1 - 3 μm diameter iron particles and (b) 10.6 μm long iron nanowires with 260 nm diameters formed in the presence of a magnetic field.

evaporate while the field was maintained. The spheres line up to form interconnected columns as depicted in Fig. 1. In addition to forming columnar structures, the nanowires of the wire-based fluids also tend to interlock with one another due to their elongated shapes.

There are a number of factors that must be considered to understand the increase in the yield stress of the nanowire-based fluids as compared to the sphere-based fluids. As noted previously, for sphere-based fluids, yield stress scales with particle size. If the increase in yield stress depended on the volume of the individual particles alone, we would expect the fluids containing the 1 - 3 µm spheres to exhibit much higher yield stresses than the wire-based fluids. (The volume of a 2 µm diameter sphere is 4.19 μm^3 and the volumes of 5.4 and 7.6 µm long wires with 260 nm diameters are 0.29 and 0.40 μm^3, respectively.) At fields below magnetic saturation, the wires have a smaller demagnetization factor and thus it is easy to understand their more sensitive response at lower magnetic fields. But above saturation, differences in magnetic saturation no longer apply.

Given that the suspensions contain the same mass of iron particles (and therefore, the same volume), the magnetic permeability of the two types of suspensions is expected be very similar. However, the local packing density of the nanowires may be slightly higher than that of the pure spheres (Bell et al., 2008), which would result in a higher local permeability and thus stronger columnar structures within the suspension. The packing density of the two nanowire distributions should be similar and we would expect the yield stress of these two fluids to be similar. However, it is apparent from Fig. 7 that the longer nanowires display a much greater yield stress than the shorter wires at the same loading. This suggests that the packing efficiency of the fluids may only play a minor role in the overall yield stress of the fluid.

The off-state viscosity of the fluids is also an important factor that must be accounted for when developing new types of MR fluids; the lower the off-state viscosity, the larger the range of achievable viscosities. The pure silicone oil used in these studies had a viscosity of 0.41 Pa·s and the off-state viscosity for the 6 vol. % fluids containing spheres was 0.66 Pa·s. The nanowire-based fluids demonstrate a similar off-state viscosity of 0.68 Pa·s for the 6 vol. % fluids, which drops to 0.50 Pa·s for the 2 vol. % fluids. However, as we now discuss, the nanowire-based fluids display a much higher degree of viscoelasticity.

Nanowire-based fluids display no discernable settling at volume fractions greater than ~4 vol. % of ~11 µm long wires after 2 months of sitting undisturbed. The exact vol. % required to effectively stop sedimentation (under vibration free conditions) depends on the length of the wires: shorter wires require higher volume percentages than longer ones. A disadvantage of the nanowire-based suspensions is that the maximum volume fraction of nanowires (< 10 vol. %) is much less than the desired 30 - 40 vol. %, achievable with spherical particles, which is necessary for high yield-stress applications. For these reasons, suspensions that contain strictly nanowires would be more useful in applications where sedimentation would be extremely detrimental or where low yield-stress is sufficient.

On the other hand, fluids employing 6 vol. % spheres displayed 79% settling in just 48 hours. The difference in the sedimentation (and the viscoelastic properties) of the two fluid types is likely a result of several factors, including nanowire entanglement, increased surface area compared to spheres, and hydrostatic and magnetic interactions between nanowires, particularly those due to remnant magnetization. Comparing the total surface area of the particles in fluids with the same volume fraction of particles, fluids containing 5.4 µm long nanowires with 260 nm diameters have more than 5 times the total surface area per volume than fluids with 2 µm diameter spheres (this difference varies little with wire length).

However, entanglement of the nanowires is likely the primary factor responsible for the differences between the sedimentation and viscoelastic properties of the two types of fluids. Entanglement occurs when the volume fraction of wires is high enough so that neighboring wires restrict the end-over-end rotational and translational motion of the wires perpendicular to the long axis (Doi & Edwards, 1978). However, this does not greatly affect the off-state viscosity of the nanowire-based suspensions under shear because the wires tend to line up and slide past one another easily, resulting in a viscosity that is similar to that of the carrier fluid at low particle concentrations (Bercea & Navard, 2000).

4. Percolation phenomena in MR fluids

The ability to predict the effective physical properties of MR-fluid composites from the known properties of the constituents would have a tremendous impact for numerous industrial processes. However, formulating an effective-medium model is complicated when the physical properties of the constituents vary greatly. In such cases, the composite material typically exhibits a phase transition at a critical volume fraction of the component of interest. The prototypical example is that of a metal-insulator composite with electrical conductivity that can change by 16-20 orders of magnitude as a critical volume of the conducting component is reached. Such a phase change in the physical properties of materials is known as a percolation transition. Numerous studies over the past few decades have focused primarily on electronic and thermodynamic transport and to some extent on the elastic and mechanical properties of materials near the critical point.

Various percolation models involving static matrices have been developed using both discrete-lattice networks and continuum networks (Stauffer & Aharony, 1994, and references therein). Each of these models attempts to determine the scaling behavior of the system using different critical exponents (s and t, in the case of conductivity networks) to describe the nature of the transition as the critical volume fraction (ϕ_c) is approached. In so-called elastic percolation networks (EPNs), a two-component mixture consists of bonds with finite elastic modulus together with completely non-rigid bonds. As ϕ_c is approached from above, the general elastic modulus (G) of an EPN is thought to vanish as (Feng et al., 1987; Deptuck et al., 1985; Sahimi, 1996),

$$G \sim (\phi - \phi_c)^f \tag{6}$$

In contrast, a superelastic percolation network (SEPN) consists of a mixture of perfectly rigid bonds and bonds with finite elastic constants. Below the critical point, the elastic moduli diverge as (Bergman, 1986),

$$G \sim (\phi_c - \phi)^{-c} \tag{7}$$

Some studies indicate that for $\phi > \phi_c$, the elastic exponent is equal to the conductivity exponent, $f = t$ (Tokita & Hikichi, 1987; Craciun et al., 1998). Other studies on the rheology of magnetic suspensions exhibiting elastic behavior suggest that f depends on concentration, varying from 1.0 to 2.26 (Kanai et al., 1992). However, most experimental measurements and theoretical models indicate that $f > t$, with typical f-values in the range of 3.5 – 4.0 (Feng et al., 1987; Deptuck et al., 1985; Sahimi, 1996), which are attributed to the higher tensorial order of EPNs. Studies of SEPN behavior in two dimensions indicate that the critical

exponent c should scale as the superconductivity exponent s (Bergman, 1986), while numerical simulations have shown c to be slightly smaller than s (Feng, 1987).

To investigate further the rheological behavior of nanowire-based MR fluids, we have systematically varied ϕ in cobalt-nanowire MR fluids and measured the dynamic yield stress for varying applied magnetic field strengths (Zimmerman et al., 2009). In doing so, we observe a percolation transition in the yield stress and find the behavior near the critical point to depend on the magnitude of the applied field.

We varied the applied magnetic field incrementally over the range of 0 – 1.0 T for samples having cobalt-nanowire volume fractions in the range $\phi = 0 - 0.06$ (note that we are using volume fraction rather than vol. %). Figure 9 shows a series of τ_y versus ϕ curves that reveal the dependence of the critical volume fraction and the transition onset on the applied field. To characterize the data we employed a normalized, two-parameter fit based on Eq. 8 and 9 using values of the yield stress extrapolated to $\phi = 0$ ($\tau_{low} \sim 5 - 12$ Pa) and far beyond ϕ_c ($\tau_{high} \sim 10^5$ Pa).

$$\tau_y = \tau_{low}\left(\frac{\phi_c - \phi}{\phi_c}\right)^{-c}, \phi < \phi_c \tag{8}$$

$$\tau_y = \tau_{high}\left(\frac{\phi - \phi_c}{1 - \phi}\right)^{f}, \phi > \phi_c \tag{9}$$

The data exhibit several trends: c decreases with increasing field, while ϕ_c increases, and f appears to be relatively constant, independent of the applied field. The extracted values of f for all field-strengths range from 1.0 to 1.2. These are intriguingly reminiscent of the
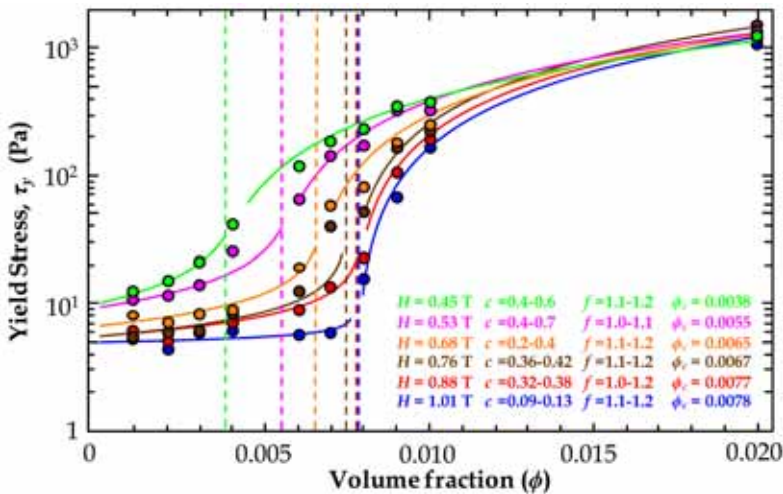

Fig. 9. The apparent yield stress (τ_y) of on-state, cobalt-nanowire MR fluids as a function of nanowire volume fraction (ϕ) for varying applied magnetic fields. The solid curves represent the best fit to expected power-law dependence given in Eq. 8 and 9. Data up to $\phi = 0.06$ was used in the analysis, but not shown for the sake of clarity near the critical point.

conductivity exponent in two-dimensional static matrices ($t \sim 1.3$) and the values of the elastic exponent ($f \sim 1.3$) found in two-dimensional, static-matrix numerical studies (Plischke & Joós, 1998; Farago & Kantor, 2000). This suggests that an MR fluid system subjected to a relatively uniform magnetic field behaves two-dimensionally, possibly because the applied field defines a preferred spatial direction for chain formation. The variation in c and ϕ_c are difficult to explain in light of known scaling models. In conductivity networks, the critical volume fraction is expected to decrease as the metal/insulator particle-size ratio decreases (Kusy, 1978), and at the same time, increase with aspect ratio due to the effect of excluded volume (Balberg et al., 1984). Yet, neither of these is a variable in the MR fluid system under study. The critical exponent, c, presumably related to the growth of elastic clusters below the transition (ferromagnetic chains in this case), varies considerably with the magnetic field. The variation in c may be describing the changes in the random reinforcement of the MR fluid by chain growth below the critical volume fraction that does not span the sample. In all likelihood, the fluid-chain morphology of the on-state MR fluids and the dynamic nature of the rheological measurements may also play a significant role in the character of the percolation transition. The importance of this issue cannot be underestimated in light of the numerous applications that exploit the MR effect.

While the values of the critical volume fraction are reasonable for nanowires having a high aspect ratio (~30), the dependence of critical volume fraction on the applied field is unexpected and likely attributed to the dynamic nature of the measurement technique and the inhomogeneities of the rheometer magnetic field. Unlike the present study, involving a dynamic-matrix fluidic system with both short-range contact and long-range magnetic interactions, the vast majority of other studies have considered static systems with short-range interactions or those involving direct particle-particle contacts. In future studies, we will vary the nanowire aspect-ratio, use other ferromagnetic materials (e.g., iron and nickel), and employ quasistatic, rather than dynamic measurements, to help separate these issues from the underlying physical mechanisms.

5. Dimorphic magnetorheological fluids

Dimorphic MR fluids were conceived as a way to realize the benefits of both nanowire-based and conventional MR fluids (Ngatu et al., 2008). In particular, we wanted to synthesize an MR fluid having low sedimentation properties yet having sufficiently high particle-loading to achieve high yield stress. We investigated the rheology and sedimentation stability of these dimorphic fluids, which substitute a given percentage of spheres within a conventional MR fluid for nanowires. For these studies, we used iron spheres of diameter 8 ± 2 µm and iron nanowires with diameters of 230 nm and lengths ranging 7.6 ± 5.1µm suspended in a 0.18 Pa · s silicone oil. Samples were generated for total particle loadings of 50, 60, and 80 wt. % combined with nanowire loading from 0 to 8 wt. % in 2 wt. % increments. This resulted in off-state viscosities for fluids with a total loading of 80 wt. % ranging from 1.3 Pa · s for the pure sphere fluids to 4.4 Pa · s for the 8 wt. % nanowire-substituted dimorphic fluids.

Dimorphic MR fluids with moderate particle loading of 50 and 60 wt. % displayed yield-stress behavior very similar to conventional fluids as seen in Fig. 10. However, we observe slight differences in the yield-stress of dimorphic MR fluids at 80 wt. %. At low field strengths, a slight increase in yield stress with increasing wire substitution was observed, consistent with the enhanced response observed in pure nanowire MR fluids at lower field

strengths. At moderate field strengths there were no differences in performance. At high fields approaching the magnetic saturation of the particles, there was an increase in yield-stress of 10% for 2 wt. % substituted dimorphic fluids. Yet, with a further increase in nanowire substitution we observe a ~5 % *decrease* for 8 wt. % substituted dimorphic fluids. This was hypothetically explained by considering the chain structures formed in conventional fluids compared to those formed by dimorphic fluids. At higher loadings, SEM micrographs showed that the wires began to interfere with the columnar structure of the on-state fluids.

Sedimentation stability analysis of dimorphic fluids showed drastic improvements across all ranges of particle loading. Time constraints were a factor in this study since only one sample could be tested at a time and each test required a minimum of one month. Thus, not all samples underwent both rheological and sedimentation tests. For fluids in the moderate particle loading ranges of 50 and 60 wt. %, only one conventional and one dimorphic sample were tested so that the more highly-loaded fluid samples of 80 total wt. %, which are more commonly employed throughout industry, could undergo more extensive testing.

Sedimentation tests of the moderately loaded fluids showed a decreased (order of magnitude lower) sedimentation velocity when comparing 50 wt. % conventional fluids to dimorphic fluids with 6 wt. % substitution, as well as 60 wt. % conventional fluids to 8 wt. % substituted dimorphic fluids. Dimorphic fluids with a total loading of 80 wt. % also showed
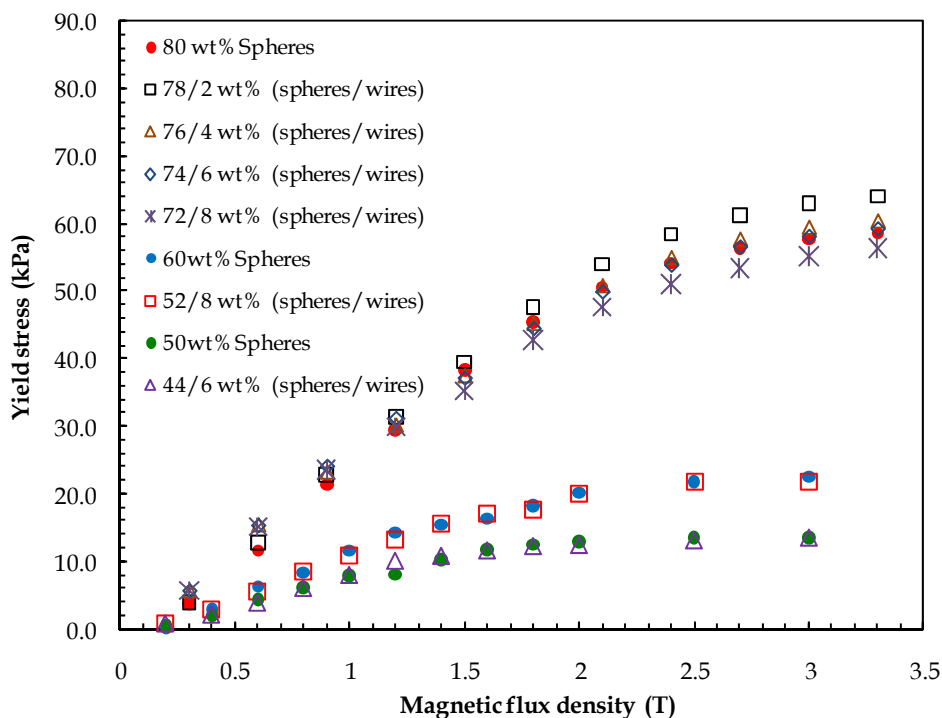

Fig. 10. Yield stress versus magnetic field for conventional sphere-based fluids and for dimorphic fluids of the same total particle loading.

a significant sedimentation rate decrease. The rate of 2 wt. % substituted fluids decrease by a factor of two, while the rate of 4 wt. % substituted dimorphic fluids displayed an order of magnitude decrease. Similarly, the difference in the degree of sedimentation between conventional and dimorphic fluids for the same samples showed a total sedimentation decrease of 50% in 50 wt. % loaded fluids and an 80% decrease in 60 wt. % loaded fluids. The 80 wt. % fluids showed a decrease in total sedimentation of 40% in 2 wt. % substituted fluids and 60% in 4 wt. % substituted fluids. Results of the sedimentation tests are summarized in Table 1.

Composition	Sedimentation Velocity [µm/s]	Sedimentation Percentage (%)
50 wt. % spheres	1.9	72.9
44 wt. % spheres + 6 wt. % wires	0.036	23.4
60 wt% spheres	0.86	66.7
52 wt% spheres + 8 wt% wires	0.017	14.0
80 wt% spheres	0.0254	14.8
78 wt% spheres + 2 wt% wires	0.0122	8.8
76 wt% spheres + 4 wt% wires	0.0021	5.7

Table 1. The sedimentation velocity and percentage sedimentation of iron-based dimorphic fluids containing various wt. % substitutions of spheres by nanowires.

In summary, the benefits of using dimorphic MR fluids over conventional MR fluids are effected by the heterogeneous chain structures formed in dimorphic fluids - the nanowires appear to structurally support the chains that are primarily formed by spheres (Ngatu et al., 2008). However, as wire substitution is increased, there appears to be a threshold reached where the wires begin to interfere with the columnar structures formed by the spheres resulting in a lower yield stress at higher wire substitution.

6. Magnetorheological elastomers

Elastomers (i.e., silicone, polyurethane, natural rubber, etc.) have been commonly used for "passive" shock and vibration attenuation, yet passive damping performance is limited due to the fixed viscoelastic properties of these materials. To overcome these performance limitations, magnetorheological elastomers (MREs) have been recently introduced and are being actively studied. MREs are multifunctional materials as they can also be used as sensors or actuators similar to other controllable, active-damping materials such as piezoelectrics, magnetostrictives, electroactive polymerics, and so on. However, in contrast to other active-damping materials, MREs can operate in a passive mode as well. MREs operate in the active mode by application of a variable applied magnetic field that changes the frequency-dependent elastic modulus.

We examined both the static and dynamic character of nanowire-based MRE composites (Song et al., 2009a; Song et al., 2009b). These MREs were synthesized using a silicone rubber embedded with ferromagnetic particles of iron and cobalt of varying weight fraction (10, 30, and 50 wt. %). To assess the effect of particle morphology, we compared nanowire-based

MRE composites to those made with spherical particles. By means of a modified material testing machine using both static and sinusoidally-oscillating compressive loads, we measured such field-dependent properties as static and dynamic stiffness, elastic modulus, yield stress, and equivalent damping. To investigate magnetic anisotropy effects in nanowire-based MRE composites, samples were cured both in the presence and absence of a magnetic field to yield samples with nanowires both aligned and randomly oriented with respect to the field, respectively.

The static stiffness of both microsphere- and nanowire-based MRE composites increased linearly as the particle weight fraction increased as shown in Fig. 11. Iron nanowire-based MRE composites displayed a greater sensitivity to the weight fraction than that of iron microsphere-based MRE composites. The increase in stiffness of the nanowire-based MREs is primarily due to the increased surface area of nanowires compared to that of spheres. This difference in static stiffness is thus attributed to the increased contact surface area in nanowires combined with the greater compressive strength of the nanowires compared to the microspheres.

The predicted elastic modulus of the nanowire-based MRE composite was determined by the modified Halpin-Tsai equation (Halpin & Kardos, 1976) and compared with the experimental results. It was shown that the theoretical model can adequately predict the elastic properties of the composites (Song et al., 2009b).

The nanowire-based MRE composites exhibited larger specific moduli (defined as the elastic modulus over the density) than the microsphere-based samples, implying that the nanowire-based MRE composites will display enhanced performance over their heavier counterparts (i.e., lower wt. % nanowire MREs can be used in place of the heavier, higher wt. % microsphere composites). Compared to the iron nanowire-based MRE composite, the cobalt nanowire-based MRE composite displayed an even higher specific modulus.

Using the Bingham model, the total force of an MRE composite can be modeled in terms of the elastic and MR effect as follows:

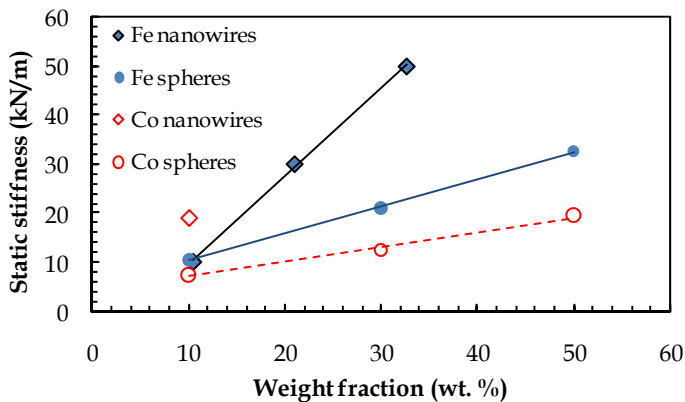$$F_{total}(t) = k_e x(t) + c_e \dot{x}(t) + F_{MRE}(t) \qquad (10)$$

Fig. 11. Measured static stiffness of the nanowire-based MRE composites versus the weight fraction of particles in the absence of magnetic field.
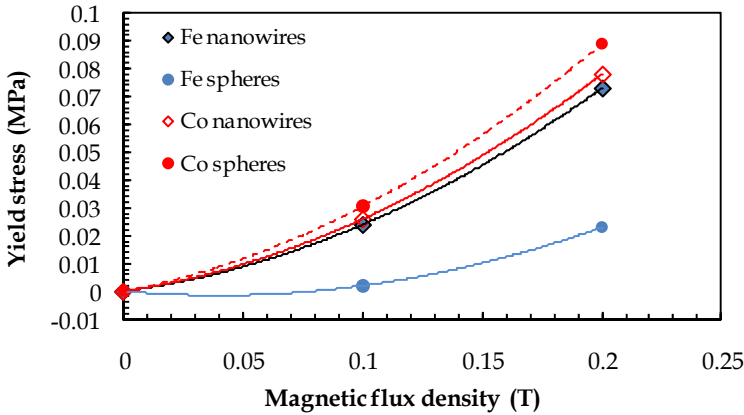
Fig. 12. The yield stress of iron and cobalt nanowire-based MRE composites versus magnetic flux density. The curves are simply a guide for the eye.

with

$$F_{MRE}(t) = \frac{4}{3} \frac{\pi r^3 \tau_y(B)}{[x_0 + x(t)]} \mathrm{sgn}[\dot{x}(t)] \tag{11}$$

Here, k_e and c_e are the stiffness and damping coefficients of the MRE composite, respectively. $F_{MRE}(t)$ is the controllable damping force at a given magnetic flux density, r is the radius of MRE composite, and x_0 and $x(t)$ are the initial position and excitation displacement, respectively. In addition, the yield stress can be represented by

$$\tau_y(B) = \alpha B^\beta \quad \text{(in MPa)} \tag{12}$$

where α and β are an empirically-determined coefficient and exponent, and B is the magnetic flux density (B) in Tesla. The yield stress of the nanowire-based MRE composites versus the magnetic flux density is shown in Fig. 12. In this figure, the yield stress was calculated from the increment of force (i.e., the difference in yield stress between 0.2 T and zero field) by using Eqs. 10-12. Similar to the yield stress behavior of MR fluids, the yield stress of the MRE composites can be modeled as a power-law function of B.

The dynamic range of the nanowire-based MRE composites was evaluated by measuring field-dependent dynamic stiffness and equivalent damping. The nanowire-based MRE composites had nearly the same dynamic stiffness; however, these composites display greater equivalent damping ranges than the microsphere-based MRE composites (Fig. 13). In addition, the 10 wt. % cobalt nanowire-based MRE composite had an increased damping capacity over that of the 10 wt. % iron nanowire-based sample.

The effect of aligned vs. nonaligned particles in the samples was observed in 10 wt. % cobalt nanowire-based MREs: aligned nanowire-based MRE composite displayed a much greater damping capacity than that of the nonaligned samples (Fig. 14).

The static stiffness of both spherical microparticle- and nanowire-based MRE composites increases monotonically as the particle-weight-fraction is increased. The nanowire-based MRE composites display a greater sensitivity to the weight fraction than that of spherical
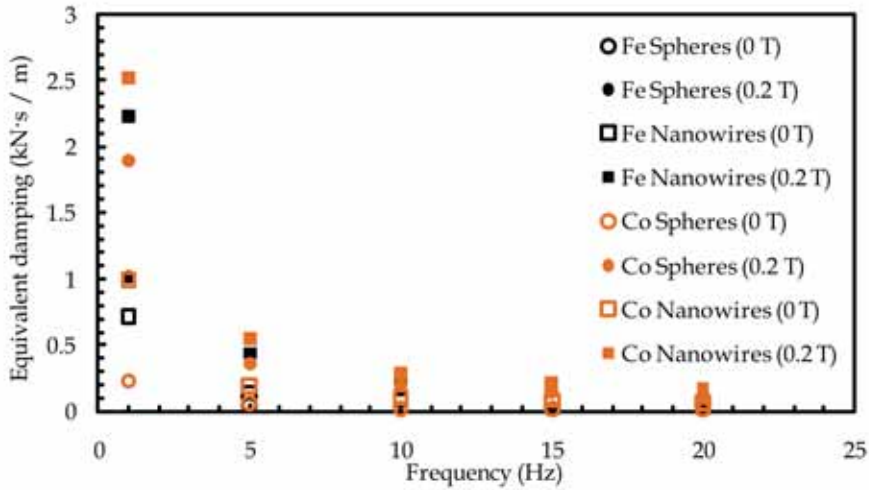
Fig. 13. Equivalent damping for 10 wt% nanowire MRE composites in the frequency domain.
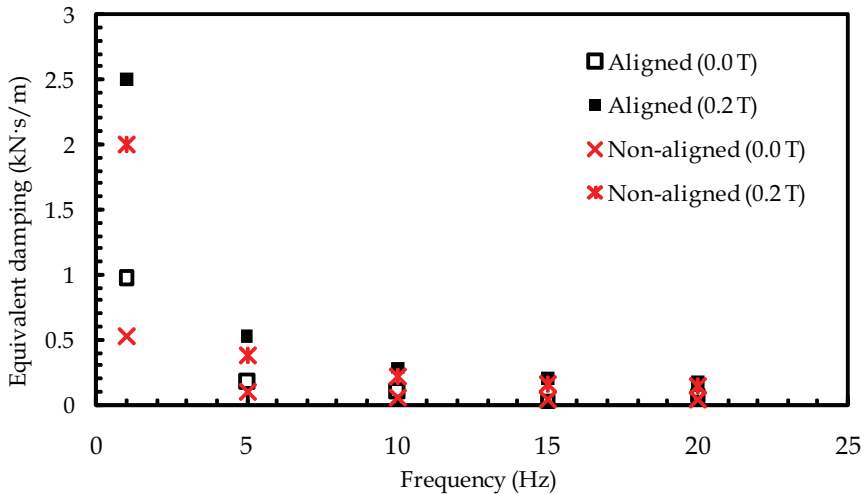

Fig. 14. Equivalent damping of the Co nanowire-based MRE composite: Aligned vs. nonaligned particles.

microparticle-based MRE composites, a result of the increased surface area of the nanowires. The nanowire-based MRE composites exhibited larger specific moduli than the microparticle-based samples, implying that the nanowire-based MRE composites having high specific moduli that can yield enhanced performance over their heavier counterparts. The nanowire-based MRE composites generated greater dynamic stiffness and equivalent damping ranges than the spherical microparticle-based MRE composites. In addition, the 10

wt% Co nanowire-based MRE composite had increased damping capacity over the 10 wt% iron nanowire-based sample.

7. Conclusions

Nanowires are well suited as model particles for the exploration of the shape- and composition-dependent properties of the suspended particles in magnetorheological fluid and elastomer composites. Two major advantages can be seen for the nanowire-based MR suspensions as compared to those that contain strictly spherical particles. The nanowire-based suspensions make for a more efficient MR fluid (higher yield stresses) at low magnetic fields allowing for more sensitive control of the fluid properties. The sedimentation velocity and the percentage of sedimentation are both greatly reduced compared to conventional MR fluids. A disadvantage of the suspensions is that the maximum volume fraction of nanowires is much less than the desired 30-40 vol. % achievable with spherical particles. For these reasons, suspensions that contain strictly nanowires would be more useful in applications where sedimentation would be extremely detrimental and low yield stresses are sufficient. Dimorphic MR fluids exhibit very attractive magnetorheological and sedimentation properties that make them feasible for an expanded set of device applications, since the higher mass loadings of conventional MR fluids can be attained. While the differences in the rheological properties of the fluids containing the spherical and nanowire particles must result from a combination of magnetic and mechanical properties, separating the details of these effects will require more in-depth experimental and theoretical studies. Further work on this new type of MR fluid will consist of examining suspensions with narrow nanowire length distributions and varying the diameters to further understand the dependency of magnetorheological and sedimentation properties on aspect ratio. In the case of nanowire-based MREs, the static stiffness was higher than that of spherical particle-based elastomers in the absence of a magnetic field at the same weight fraction due to the increased surface area of the nanowires as compared to the spherical particles. With nanowire-based MRE samples, the equivalent damping was significantly greater in the presence of a magnetic field. Future studies will include the consideration of aspect ratio dependence, as well as an exploration of the percolation transition within these unique composite materials.

8. Acknowledgements

9. References

Balberg, I.; Anderson, C. H.; Alexander, S. & Wagner, N. (1984). Excluded volume and its relation to the onset of percolation. *Physical Review B*, Vol. 30, No. 7, (October 1984) pp. 3933–3943, 0163-1829.

Bell, R. C.; Miller, E. D.; Karli, J. O.; Vavreck, A. N. & Zimmerman, D. T. (2007). Influence of particle shape on the properties of magnetorheological fluids. *International Journal of Modern Physics B*, Vol. 21, No. 28-29, (November 2007) pp. 5018–5025, 0217-9792.

Bell, R. C.; Karli, J. O.; Vavreck, A. N.; Zimmerman, D. T.; Ngatu, G. T. & Wereley, N. M. (2008). Magnetorheology of submicron diameter iron nanowires dispersed in silicone oil. *Smart Materials and Structures*, Vol. 17, No.1, (February 2008) pp. 015028-1–6, 0964-1726.

Bercea, M. & Navard, P. (2000). Shear dynamics of aqueous suspensions of cellulose whiskers. *Macromolecules,* Vol. 33, No. 16, (Aug 2000) pp. 6011–6016, 0024-9297.

Bergman, D. J. (1986). Elastic moduli near percolation in a two-dimensional random network of rigid and nonrigid bonds. *Physical Review B*, Vol. 33, No. 3, (February 1986) pp. 2013–2016, 0163-1829.

Carlson, J. D. (2003). Critical Factors for MR fluids in vehicle systems. *International Journal of Vehicle Design,* Vol. 33, No.1-3, (2003) pp. 207–217, 0143-3369.

Chaudhuri, A.; Wereley, N. M.; Kotha, S.; Radhakrishnan, R. & Sudarshan, T. S. (2005). Viscometric characterization of cobalt nanoparticle-based magnetorheological fluids using genetic algorithms. *Journal of Magnetism and Magnetic Materials*, Vol. 293, No. 1, (May, 2005) pp. 206–214, 0304-8853.

Chen, L. S. & Chen, D. Y. (2003). Permalloy inductor based instrument that measures the sedimentation constant of magnetorheological fluids. *Review of Scientific Instruments,* Vol. 74, No.7, (Jul 2003) pp. 3566–3568, 0034-6748.

Chin, B. D.; Park, J. H.; Kwon, M. H. & Park, O. O. (2001). Rheological properties and dispersion stability of magnetorheological (MR) suspensions. *Rheologica Acta*, Vol. 40, No. 3, (May, 2001) pp. 211–219, 0035-4511.

Craciun, F.; Galassi, C. & Roncari, E. (1998). Experimental evidence for similar critical behavior of elastic modulus and electric conductivity in porous ceramic materials. *Europhysics Letters*, Vol. 41, No. 1, (January 1998) pp. 55–60, 0295-5075.

Deptuck, D.; Harrison, J. P. & Zawadski, P. (1985). Measurement of elasticity and conductivity of a three-dimensional percolation system. *Physical Review Letters*, Vol. 54, No. 9, (1985) pp. 913–916, 0031-9007.

Doi, M. & Edwards, S. F. (1978). Dynamics of rod-like macromolecules in concentrated solution 1. *Journal of the Chemical Society-Faraday Transactions II,* Vol. 74, No. 3, (1978) pp. 560–570, 0300-9238.

Farago, O. & Kantor, Y. (2000). Entropic elasticity of two-dimensional self-avoiding percolation systems. *Physical Review Letters*, Vol. 85, No. 12, (September 2000) pp. 2533–2536, 0031-9007.

Feng, S.; Halperin, B. I. & Sen, P. N. (1987). Transport-properties of continuum-systems near the percolation-threshold. *Physical Review B*, Vol. 35, No. 1, (January 1987) pp. 197–214, 0163-1829.

Genç, S. & Phulé, P. P. (2002). Rheological properties of magnetorheological fluids. *Smart Materials and Structures*, Vol. 11, No. 1, (February, 2002) pp. 140–146, 0964-1726.

Halpin, J. C., & Kardos, J. L. (1976). The Halpin-Tsai equations: A review. *Polymer Engineering and Science*, Vol. 16, No. 5, (May 1976) pp. 344–352, 0032-3888.

Han, G. C.; Zong, B. Y. & Wu, Y. H. (2002). Magnetic properties of magnetic nanowire arrays. *IEEE Transactions on Magnetics*, Vol. 38, No. 5, (September 2002) pp. 2562–2564, 0018-9464.

Harland, N. R.; Mace, B. R. & Jones, R. W. (2001). Adaptive-passive control of vibration transmission in beams using electro/magnetorheological fluid filled inserts. *IEEE Transactions on Control Systems Technology*, Vol. 9, No. 2, (March 2001) pp. 209–220, 1063-6536.

Jolly, M. R.; Bender, J. W. & Carlson, J. D. (1999). Properties and applications of commercial magnetorhelogical fluids. *Journal of Intelligent Material Systems and Structures*, Vol. 10, No. 1, (January 1999) pp. 5–13, 1045-389X.

Jones, T. B. & Saha, B. (1990). Nonlinear-interactions of particles in chains. *Journal of Applied Physics*, Vol. 68, No. 2, (July, 1990) pp. 404–410, 0021-8979.

Kamath, G. M.; Wereley, N. M. & Jolly, M. R. (1999). Characterization of magnetorheological helicopter lag dampers. *Journal of the American Helicopter Society*, Vol. 44, No. 3, (July 1999) pp. 234–248, 0002-8711.

Kanai, H.; Navarrette, R. C.; Macosko, C. W. & Scriven, L. E. (1992). Fragile networks and rheology of concentrated suspensions. *Rheologica Acta*, Vol. 31, No. 4, (1992) pp. 333–344, 0035-4511.

Kanu, R. C. & Shaw, M. T. (1998). Enhanced electrorheological fluids using anisotropic particles. *Journal of Rheology*, Vol. 42, No. 3, (May-June, 1998) pp. 657–670, 0148-6055.

Klingenberg, D. J. (2001). Magnetorheology: Applications and challenges. *American Institute of Chemical Engineers (AIChE) Journal,* Vol. 47, No. 2, (February, 2001) pp. 246–249, 0001-1541.

Kordonski, W. I.; Shorey, A. B. & Tricard, M. (2006). Magnetorheological jet (MR Jet (TM)) finishing technology. *Journal of Fluids Engineering – Transactions of the ASME*, Vol. 128, No. 1, (January 2006) pp. 20–26, 0098-2202.

Kusy, R. P. (1977). Influence of particle size ratio on the continuity of aggregates. *Journal of Applied Physics*, Vol. 48, No. 12, (December 1977) pp. 5301–5306, 0021–8979.

Kuzhir, P.; Lopez-Lopez, M. T. & Bossis, G. (2009). Magnetorheology of fiber suspensions. II. Theory. *Journal of Rheology,* Vol. 53, No. 1, (January/February 2009) pp. 127–151, 0148-6055.

López-López, M. T.; Kuzhir, P. & Bossis, G. (2009) Magnetorheology of fiber suspensions. I. Experimental. *Journal of Rheology*, Vol. 53, No. 1, (January/February 2009) pp. 115–126, 0148-6055.

Ngatu, G. T. & Wereley, N. M. (2007). Viscometric and sedimentation characterization of bidisperse MR fluids. *IEEE Transactions on Magnetics*, Vol. 43, No. 6, (June 2007) pp. 2474–2476, 0018-9464.

Ngatu, G. T.; Wereley, N. M.; Karli, J. O. & Bell, R. C. (2008). Dimorphic magnetorheological fluids: exploiting partial substitution of microspheres by nanowires. *Smart Materials and Structures*, Vol. 17, No. 4, (August 2008) pp. 045022-1–8, 0964-1726.

Nishiyama, H.; Katagiri, K.; Hamada, K.; Kikuchi, K.; Hata, K.; Sang-Kyu, P. & Nakano, M. (2005). Evaluations of cluster structure and magneto-rheology of MR suspensions.

International Journal of Modern Physics B, Vol. 19, No. 7-9, (April 2005) pp. 1437–1442, 0217-9792.

Phulé, P. P. & Ginder, J. M. (1998). The materials science of field-responsive fluids. *MRS Bulletin*, Vol. 23, No. 8, (August 1998) pp. 19–21, 0883-7694.

Plischke, M. & Joós, B. (1998). Entropic elasticity of diluted central force networks. *Physical Review letters*, Vol. 80, No. 22, (June 1998) pp. 4907–4910, 0031-9007.

Poddar, P.; Wilson, J. L.; Srikanth, H.; Yoo, J. H.; Wereley, N. M.; Kotha, S.; Barghouty, L. & Radhakrishnan, R. (2004). Nanocomposite magneto-rheological fluids with iniformly dispersed Fe nanoparticles. *Journal of Nanoscience and Nanotechnology*, Vol. 4, No. 1-2, (January-Feburary 2004) pp. 192–196, 1533-4880.

Qi, Y.; Zhang, L. & Wen, W. (2003). Anisotropy properties of magnetic colloidal materials. *Journal of Physics D-Applied Physics*, Vol. 36, No. 1, (January 2003) pp. L10–L14, 0022-3727.

Ramallo, J. C.; Johnson, E. A. & Spencer Jr., B. F (2002). "Smart" base isolation systems. *Journal of Engineering Mechanics*, Vol. 128, No. 10, (October 2002) pp. 1088–1099, 0733-9399.

Rosenfeld, N.; Wereley, N. M.; Radakrishnan, R. & Sudarshan, T. S. (2002). Behavior of magnetorheological fluids utilizing nanopowder iron. *International Journal of Modern Physics B*, Vol. 16, No. 17-18, (July, 2002) pp. 2392–2398, 0217-9792.

Sahimi, M. (1996). Linear and nonlinear, scalar and vector transport processes in heterogenous media: Fractals, percolation, and scaling laws. *Chemical Engineering Journal*, Vol. 64, No. 1, (October 1996) pp. 21–44, 0923-0467.

Sanchis, A.; Sancho, M.; Martínez, G.; Sebastián, J. L. & Muñoz, S. (2004). Interparticle forces in electrorheological fluids: effects of polydispersity and shape. *Colloids and Surfaces A-Physicochemical and Engineering Aspects*, Vol. 249, No. 1-3, (November 2004) pp. 119–122, 0927-7757.

Song, H. J.; Wereley, N. M.; Bell, R. C.; Planinsek, J. L. & Filer II, J. A. (2009a). Field dependent response of magnetorheological elastomers utilizing Fe spherical particles versus Fe nanowires. *Journal of Physics: Conference Series*, Vol. 149, (March 2009) pp. 012097-1–4, 1742-6596.

Song, H. J.; Padalka, O.; Wereley, N. M. & Bell, R. C. (2009b). Impact of nanowire versus spherical microparticles in magnetorheological elastomer composites. *Proceedings of the 50th AIAA/ASME/ASCE/AHS/ASC Structures, Structural Dynamics and Materials Conference*, 9781615671380, Palm Springs, CA, May, 2009, Curran Associates, Inc., Red Hook, New York.

Stauffer, D. & Aharony, A. (1994). *Introduction to Percolation Theory, Revised 2nd Edition*, Taylor and Francis Inc., 0748402535, Philadelphia.

Sun, L.; Hao, Y.; Chien, C. L. & Searson, P. C. (2005). Tuning the properties of magnetic nanowires. *IBM Journal of Research and Development*, Vol. 49, No. 1, (January 2005) pp. 79–102, 0018-8646.

Tokita, M. & Hikichi, K. (1987). Mechanical studies of sol-gel transition: universal behavior of elastic modulus. *Physical Review A*, Vol. 35, No. 10, (May 1987) pp. 4329–4333, 1050-2947.

Weiss, K. D.; Nixon, D. A.; Carlson, J. D. & Margida, A. J. (1997). Thixotropic magnetorheological materials. *US Patent* 5 645 752.

Wereley, N. M.; Chaudhuri, A.; Yoo, J. H.; John, S.; Kotha, S.; Suggs, A.; Radhakrishnan, R.; Love, B. J. & Sudarshan, T. S. (2006). Bidisperse magnetorheological fluids using Fe particles at nanometer and micron scale. *Journal of Intelligent Material Systems and Structures*, Vol. 17, No. 5, (May, 2006) pp. 393–401, 1045-389X.

Yin, J. B. & Zhao, X. P. (2006). Titanate nano-whisker electrorheological fluid with high suspended stability and ER activity. *Nanotechnology*, Vol. 17, No. 1, (January 2006) pp. 192–196, 0957-4484.

Zimmerman, D. T.; Bell, R. C.; Filer II, J. A.; Karli, J. O. & Wereley, N. M. (2009). Elastic percolation transition in nanowire-based magnetorheological fluids. *Applied Physics Letters*, Vol. 95, No. 1, (July 2009) pp. 014102-1–3, 0003-6951.

Zipser, L.; Richter, L.; Lange, U. (2001). Magnetorheologic fluids for actuators. *Sensors and Actuators A*, Vol. 92, No. 1-3, (August 2001) pp. 318–325, 0924-4247.